Journal of Structural Geology 31 (2009) 1350–1364

Contents lists available at ScienceDirect

Journal of Structural Geology

journal homepage: www.elsevier.com/locate/jsg

Modelling of porphyroclasts in simple shear and the role of stress variations at grain boundaries

Christopher J.L. Wilson [a,*], Lynn Evans [a], Claudio Delle Piane [b]

[a] School of Earth Sciences, The University of Melbourne, Melbourne, Victoria 3010, Australia
[b] CSIRO Petroleum Resources, Australian Research Centre, Kingston 6151, Western Australia

ARTICLE INFO

Article history:
Received 5 January 2009
Received in revised form
22 July 2009
Accepted 1 August 2009
Available online 11 August 2009

Keywords:
Two-phase composites
Microstructure
Micro-mechanisms
Simple shear

ABSTRACT

Grain-scale numerical experiments involving simple shear of a two-phase non-linear viscous material are described and compared with mineral fish or lozenge-shaped porphyroclasts, such as muscovite. Two types of 2D models are considered; either a single elongate grain or two parallel elongate grains, in both cases supported by a weaker polygonal grain matrix. The relative viscosities of the contrasting grain structures were systematically varied, allowing us to observe the effects of non-linear viscous rheology on the resulting microstructure and flow patterns. The results show that the finite rotation of the hard elongate grain was similar within any one experiment, but was largely influenced by viscosity contrast, the geometry of the model and the imposed shear strain. Models involving single elongate hard grains show increasing instability at their ends and less strain compatibility with the deforming matrix grains, as the viscosity contrast is increased. In the paired grain models the greatest variation in the matrix grain microstructure is seen in the region where the two hard grains are oriented at a high-angle to the direction of shear. Finally, we consider the changes in intragranular stress by comparing microstructural observations using different viscosities with the distribution of stress in space and during progressive shear. In the plane approximately parallel to the maximum principal stress direction (σ_1), a localised change of stress occurs across and along the interface between the hard and soft grains. Variations in the mean stress at these boundaries are directly attributable to changes in the minimum principal stress. We propose that with shear strains greater than $\gamma = 2$ it is the minimum principal stress that can control diffusion processes at the grain boundary rather than mean stress. In conclusion we suggest that our models have the potential for providing useful insights into why metamorphic reactions can occur at the interface between a porphyroclast and matrix at high shear strains and how stress distribution can control the initiations of such reactions.

© 2009 Elsevier Ltd. All rights reserved.

1. Introduction

Shearing processes in two-phase systems, such as quartz–muscovite and calcite–muscovite bearing rocks, in the middle to lower crust, involve the rotational behaviour of rigid particles in a deforming matrix. In these rocks, characteristic microfabrics develop via a combination of dynamic recrystallisation and grain growth, driven by chemical reactions, reduction of boundary energy or reduction of stored defect energies (Evans et al., 2001; Herwegh and Jenni, 2001). The relation between a rotating object and its matrix has long been of interest in the geosciences and material sciences as a tool to quantify the amount of strain recorded in a rock. Jeffery (1992) published a seminal work on this topic and this work has formed the basis of numerous theoretical, analogue and numerical investigations of rigid object kinematics in deforming rocks (Johnson, 2008 and references therein; Marques et al., 2007). Some observations in both naturally and experimentally deformed rocks are not well described by the analytical theory of Jeffery (1992). For example, Lister and Snoke (1984) and earlier workers such as Eisbacker (1970) noted that elongate muscovites in very-high-strain rocks (mylonites) commonly form mineral "fish" or lozenge-shaped porphyroclasts that undergo microboudinage (e.g. Fig. 1a, b). Whereas, coexisting biotite grains are readily deformed and recrystallise (Bell and Wilson, 1981; Johnson et al., 2004) and do not normally develop as "mica fish".

Fish shaped structures have also been generated during simple shear from square objects, in a more competent matrix, in the finite element models of Treagus and Lan (2003). Analogue experiments using rigid objects in a weak matrix undertaken by ten Grotenhuis et al. (2002) and Ceriani et al. (2003) suggest that slip occurs along

* Corresponding author. Tel.: +61 3 8344 6538; fax: +61 3 8344 7761.
E-mail address: cjlw@unimelb.edu.au (C.J.L. Wilson).

0191-8141/$ – see front matter © 2009 Elsevier Ltd. All rights reserved.
doi:10.1016/j.jsg.2009.08.001

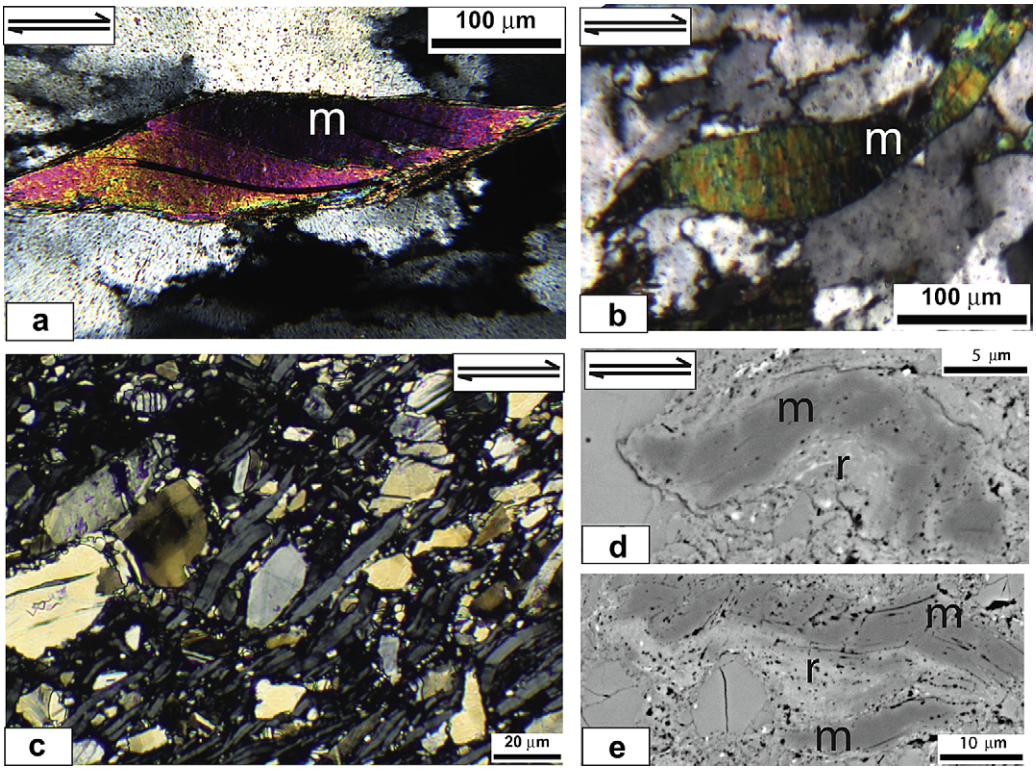

Fig. 1. Muscovite microstructures that relate to the evolution of mica fish. (a) Micrograph of single muscovite mica (m) in a recrystallised quartz matrix from the Risfjallet, shear zone, Sweden (Wilson, 1975). Some of the deformation may be accommodated by slip on the (001) cleavage. (b) Muscovite (m) grains in quartz matrix from Risfjallet shear zone with ends of the muscovite fish becoming buckled. (c) Calcite–muscovite sample deformed in a torsion experiment (PO781 of Delle Piane et al., 2009) at $T = 627\ ^{\circ}C$, shear strain rate $6 \times 10^{-5}\ s^{-1}$ and bulk shear strain of $\gamma = 1$. The muscovite grains are located between the twinned calcite grains and have been rotated and buckled during the sinistral shear and there is no reaction phase. (d, e) SEM micrographs from torsion experiment PO754 ($\gamma = 4.5$; $T = 727\ ^{\circ}C$) of Delle Piane et al. (2009) showing deformed muscovite (m = dark phase) with reaction zone (r = light phase), that contains anorthite and kalsilite, adjacent to the inner arc of the deformed muscovite grains in a matrix of recrystallised calcite.

discrete shear zones in the matrix away from the object or at the interface and may promote the development of oblique stable positions of elongate particles. These and other numerous studies summarised by Mancktelow (2002) suggest that the lozenge-shaped particles could promote slip on the long straight interface and the deforming matrix. Another possibility proposed by ten Grotenhuis et al. (2003), is that the tips of mica fish are isoclinally folded and break off along the hinge of these microfolds.

In addition to the above studies, that suggest there is a component of brittle fracturing, many experimental studies have reproduced 'fish' like objects in a deformed matrix. These are accompanied by changes in the strength contrast between a weak and strong phase, which in turn influences the deformation mechanism (Holyoke and Tullis, 2006). In particular, in many of the high shear strain experiments in bimineralic rocks, it has been demonstrated that there is a switch in deformation mechanisms that may involve a small amount of interstitial melt (Dell'Angelo et al., 1987; Dell'Angelo and Tullis, 1988; Jackson et al., 2006) together with a transition from dislocation creep to diffusion creep (Barnhoorn et al., 2005). In large-strain experiments on calcite–quartz aggregates, Rybacki et al. (2003) reported heterogeneous deformation and the stress exponent increased substantially with increasing quartz content and this was accompanied by a metamorphic reaction that produced wollastonite. Delle Piane et al. (2009) have reported similar chemical reactions between calcite and muscovite porphyroclasts. The spatial distribution between these phase transformations or metamorphic reactions cannot be due to initial variation in composition, nor is temperature variation a likely explanation for these observations. However, as pointed out by Casey (1980) and Mancktelow (2002), stress gradients associated with heterogeneous strain can be significant, even when the magnitudes of deviatoric stresses are small. Gradients in the mean stress, could produce a positive feedback, but the establishment of these gradients during the formation of a porphyroclast has only received limited attention (e.g. Tenczer et al., 2001; Johnson et al., 2004).

In the two-phased experiments of Delle Piane et al. (2009) there is a complex interplay between the lower shear strength in the calcite compared to the stronger muscovite (Fig. 1c). This produces mica fish, folded and boudinaged muscovite and metamorphic reactions (Fig. 1d, e). Delle Piane et al. (2009) observed that at shear strains (γ) greater than 2 and decreasing shear stress conditions, extension sites are preferential loci that favour the mobility of elements and the growth of a new phase. They also suggest mineral growth via volume diffusion has to overcome the influence of pressure differences between mean stress, i.e. the algebraic mean of the principal stresses (Means, 1976), and the minimum principal stress σ_3.

In this contribution, we show how numerical modelling can be used to gain deeper insights into the evolution of tabular grains in a polycrystalline matrix and the role of stress in controlling the sites for metamorphic reactions. Specifically it focuses on the spatial and temporal patterns of instantaneous and cumulative deformation at the grain scale. We concentrate on varying two input parameters (Table 1), the stress exponent (n) and the viscosity strength constant (vr), which equate to the viscosity in linear viscous systems (Jessell et al., 2009). This allows us to investigate grain-scale processes that may lead to localisation of deformation and phase transformation around a harder object, namely the interaction between a weak and strong mineral deformed by viscous flow. We utilise the approach of Jessell et al. (2005, 2009) of using the Elle software to simulate the type of microstructures observed in

Table 1
The variation in initial orientation, viscosity ratio (vr), stress exponent (n) and bulk shear strain (γ) that relates the simple shear numerical experiments to figure numbers.

Figure number	Hard grain(s) initial orientation to shear plane	Viscosity ratio vr	Stress exponent n	Bulk shear strain γ
4a–c	Single perpendicular	10, 20, 30	1	5, 10, 15
4d, 4	Single perpendicular	40	1	5, 10, 15, 17.5
6	Single perpendicular	10, 20, 40	3	2.5
7c	Paired perpendicular	10	1	3, 6
7d	Paired perpendicular	20	1	3, 6
7e, f	Paired perpendicular	40	1	3, 6, 9
8c	Paired parallel	10	1	3, 6
8d	Paired parallel	20	1	3, 6
9e, f	Paired parallel	40	1	3, 6, 9
9a	Paired perpendicular	20	1	3
9b, c	Paired perpendicular	20	3	3
9d, e	Paired perpendicular	20	5	3

naturally occurring high-strain rocks such as mylonites (Lister and Snoke, 1984; ten Grotenhuis et al., 2003) or high-strain experiments described by Delle Piane et al. (2009). Finally, we cast the results of our modelling in a more general context to modify current notions on the relationship between diffusion processes and the state of stress in a poly-phase grain aggregate.

2. Modelling procedure and configuration

Two-dimensional grain-scale numerical simulations have been successful in reproducing some aspects of microstructural development during strain localisation (Mancktelow, 2006; Johnson et al., 2004; Zhang et al., 1996). However, the localised incompatibility of strain across grain boundaries is bound to create significant stresses in the vicinity of these boundaries (Tullis et al., 1991; Wilson and Zhang, 1994). This will affect the stored elastic energy both promoting reactions as described by Delle Piane et al. (2009) and enhancing the kinetics to produce melting (Jackson et al., 2006; Wilson et al., 1996). In the geological literature several approaches have been developed to model heterogeneous flow of coarse grained, polyphase rocks and some of the earlier studies have been summarised by Handy et al. (1999). With these methods the evolution of a material can be related to the appropriate mechanical and physical conditions. In most ductile shear zones the minerals making up the matrix deform by one or more thermally activated deformation mechanisms that are associated with both non-linear (dislocation creep) and linear (diffusion-accommodated processes) (Mancktelow, 2006; Wheeler and Ford, 2008). The deformation involving such mechanisms is therefore termed viscous flow and in this contribution we use the non-linear viscous finite element code BASIL (Barr and Houseman, 1996; Houseman et al., 2008) to model two non-linear viscous phases one strong and one weak.

To construct the numerical experiments we use the simulation platform Elle (Jessell et al., 2001; Bons et al., 2008). The grain structure is represented as polygons (Fig. 2a) that are defined by nodes linked by straight segments and these polygons may be assigned physical and chemical attributes. In the experiments described here, the polygons are inferred to represent calcite and muscovite crystals, and the only active process is simple shear deformation of the crystals that is modelled by moving the nodes. The velocity and direction for each node movement are calculated using BASIL, which computes internal stress distribution, pressure, creep strain rates and displacements rates. BASIL is a 2D finite element code that assumes a constitutive law, relating deviatoric

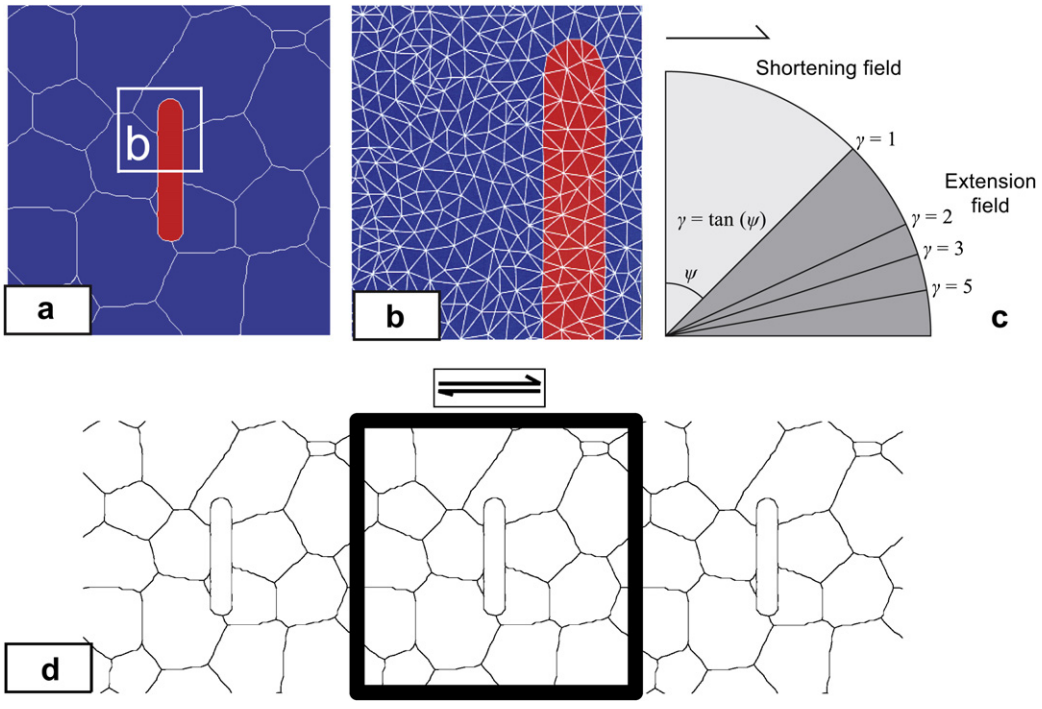

Fig. 2. The initial microstructure and orientation regimes that govern the sense of grain rotation. (a) A single grain, to simulate a muscovite, in a weaker matrix. The matrix grains are polygons representing calcite or quartz and the rod-shaped grains represent muscovite. (b) Portion of the Delaunay triangulation mesh, white box in (a) adapted to grain boundaries used for finite element calculations at each time step. (c) The dextral shear fields described in these experiments. Grains lying in the shortening field, that is the perpendicular orientation, are rapidly rotated into the extensional field after shear strain increments of $\gamma \geq 1$. (d) The square represents the area observed in a model run, with the microstructure continuing across the two vertical boundaries; this can produce the wrapping, across vertical boundaries during the dextral simple shear, particularly in the microstructures observed at higher strains (e.g. Figs. 7 and 8).

stress and strain rate, which can be cast in terms of an incompressible, possibly non-linear, viscous deformation:

$$\tau_{ij} = \boldsymbol{B}\dot{\boldsymbol{E}}^{((1/n)-1)}\,\dot{\epsilon}_{ij} = 2\eta\dot{\epsilon}_{ij} \quad (1)$$

where τ_{ij} is the deviatoric stress, B is a material constant, $\dot{E}$ is the second invariant of the strain rate tensor, n is the stress exponent, $\dot{\epsilon}_{ij}$ is the strain rate and η is the viscosity (Ranalli, 1995). When both materials deform under the same stress and B is set to 1 for the matrix, the viscosity contrast is given by:

$$\eta = B^n \quad (2)$$

This viscosity contrast is described by Tenczer et al. (2001) and Eq. (2) allows us to simulate the rheology as applied in the torsion experiments of Delle Piane et al. (2009) and to vary the viscosity contrasts between the polygons. For simple experiments involving only viscous deformation, the BASIL program could be used alone but, as with all finite element codes, the strain that can be achieved is limited to the point where an element is flattened, often at $\gamma < 2$. By using BASIL within the Elle framework and iteratively applying small timesteps of deformation while regridding between steps, we are able to simulate larger strains, $\gamma > 10$.

The finite element mesh for the deformation calculation may be created by the mesh generation code, Triangle (Shewchuk, 2002), which uses a Delaunay triangulation (Fig. 2b). The triangulation is constrained not to cross the grain boundaries and thus allows a better resolution of properties at the phase boundaries (Evans et al., 2008). In this paper, we use the convention that extensional (tensile) stresses are given positive values, which are opposite to the usual geological convention, and compressional values are negative.

2.1. Starting model and assumptions

The initial microstructure for these two-dimensional experiments is a unit square with periodic horizontal and vertical boundaries. The horizontal boundaries are fixed during the deformation step but the horizontal periodicity is maintained. The input structure consists of two phases, a weaker matrix of mainly equant grains and either a stronger single (Fig. 2) or paired elongated grains representing muscovite platelets. For these experiments, only the boundaries between the phases are significant grain boundaries while the intraphase boundaries act as markers that track stress and strain.

One experimental run consists of the iterative application of small ($\gamma = 0.05$) increments of dextral simple shear deformation to a model with initially square boundaries. Since the BASIL code supports periodic boundary conditions across the vertical sides of our model (Jessell et al., 2009), we were able to make use of the code within Elle to maintain a constant square boundary at the end of each increment of deformation (Fig. 2c). As the grain moves from the shortening into the extensional strain field (Fig. 2d) there can be an apparent wrap around of grains in the horizontal plane.

2.2. Assumptions

The viscosity strength contrast is the parameter that differentiates the two phases and the ratio (vr) remains fixed and constant within each phase throughout the deformation. It is likely that the viscosity varies in the matrix with areas of strain-driven grain reduction having lower viscosity (Jessell et al., 2005) while there may be strain softening or hardening due to deformation of the porphyroclast lattice.

The deformation is the only process acting on the grain boundaries and we ignore grain size reduction due to recrystallisation, grain boundary migration or metamorphic reaction. The interfaces are cohesive with no slip on grain boundaries. The deformation calculations assume area is conserved so there is no increase due to dilation or decrease with void removal. Although our numerical model is not 3D Arbaret et al. (2001) have shown that, for these simple rotational experiments, the behaviour is well described by 2D simulations.

2.3. Effective viscosity contrast with reference to calcite and muscovite

The flow used in these models is viscous with a stress exponent, n, in the range 1–5 (Table 1). These values of n are commonly applied to lithospheric rocks in the literature, for example, Stüwe (2007) suggests 2–4 and Passchier and Trouw (2005) less than or equal to 5. In this paper we will relate the new findings from the numerical simulations to the experimental work presented by Delle Piane et al. (2009), where a synthetic aggregate of calcite and muscovite was deformed to large strains at high temperature. We have selected some representative experimental values from high-temperature deformation tests on calcite and muscovite in estimating the effective viscosity ratio (η) between the two mineral components (Table 2).

There is an extensive set of experimental data on the high-temperature deformation behaviour of calcite. Data are available for small strain coaxial tests on single crystal (de Bresser and Spiers, 1997), fine-grained synthetic aggregates (e.g. Walker et al., 1990) and natural marbles (Schmid et al., 1980; Rutter, 1995; Ter Heege et al., 2002). Also experiments have been performed to large strain using the torsion technique on natural Carrara marble (Pieri et al., 2001; Barnhoorn et al., 2004; Delle Piane and Burlini, 2008) at conditions of temperature, pressure and strain rate that are mimicked in the dataset presented in this work. Previous experiments are reproducible giving very small variance and therefore a reliable dataset. Based on the experimental data of Barnhoorn et al. (2004), the viscosity of Carrara marble at 727 °C, 300 MPa and strain rate of $3 \times 10^{-4}\ s^{-1}$ can be calculated as being approximately 1.37×10^{11} Pa s (Table 2).

There have also been numerous experimental studies on the deformation of mica single crystals (Etheridge et al., 1973; Mares and Kronenberg, 1993), and muscovite aggregates (Mariani et al., 2006). Using the experimental dataset of Mariani et al. (2006) we estimate that muscovite at conditions of 700 °C and strain rate of $1.5 \times 10^{-4}\ s^{-1}$ has a viscosity of 4×10^{-11} Pa s. Neglecting the small temperature and strain rate differences between the two experimental datasets, one can estimate the viscosity ratio as:

$$\frac{\eta M}{\eta C} = 2.9 \quad (3)$$

where ηM is the viscosity of muscovite and ηC is the viscosity of calcite. Using the strain rate values of $1.2 \times 10^{-5}\ s^{-1}$ and $6 \times 10^{-5}\ s^{-1}$ for muscovite and calcite (Table 2) the viscosity ratio rises to a value of 7.2. These results assume the absence of any metamorphic reaction, and the hard grain (mica component) is

Table 2
Experimentally derived viscosity values for muscovite (Mariani et al., 2006) and calcite (Barnhoorn et al., 2004).

T (°C)	Strain rate (s^{-1})	Flow stress (MPa)	Viscosity (Pa s)
Muscovite			
700	1.20E-05	68	5.67E+12
700	1.50E-04	60	4.00E+11
Calcite			
727	6.00E-05	47	7.83E+11
727	3.00E-04	41	1.37E+11

assumed immobile to diffusion processes, which in reality is not the case as illustrated by Delle Piane et al. (2009).

Reactions between calcite and muscovite were only identified by Delle Piane et al. (2009) when the bulk shear strain is greater than $\gamma = 2.5$ and when the strength of the deforming aggregate was quasi-steady. Chemical profiles from the calcite matrix across any muscovite (Fig. 3a, b) display sharp changes in Al, K and Ca content. The cores of the muscovite grains present flat Al-rich, K-rich profiles and Ca-poor profiles, whereas, their boundaries are characterised by a transitional chemical change that probably correspond to the reaction products anorthite and kalsilite identified by Delle Piane et al. (2009). In curved muscovite grains the transition is always asymmetric with a narrow zone (2–4 μm wide) on the outer arc and a wider zone (8–12 μm wide) in the concave inner arc (Fig. 3c, d). Planar muscovite grains may also have narrow transitional but symmetrical fringes (~2 μm wide). This fringing on the muscovite implies that there was a transfer of components during deformation.

3. Single porphyroclast with contrasting matrix viscosities

The first set of models embedded a single hard elongate grain, initially perpendicular to the shear plane, in a weaker matrix and applied a dextral simple shear (Fig. 4). With a viscosity contrast of $vr = 10$ there is both progressive rotation and extension of the matrix grains (Fig. 4) with increasing shear strain (Fig. 4a). With increased viscosity ratios (Fig. 4b–d), the hard grain does not elongate as much as the matrix grains. In this situation there is partitioning of deformation, while maintaining perfect cohesion between the hard grain and the matrix grains; unlike the analogue models of ten Grotenhuis et al. (2002) and Ceriani et al. (2003). The deformation is mainly elongation and the porphyroclast has a larger aspect ratio when it has rotated into the shear direction. As the short axis is small, it does not provide much resistance to the shear flow and therefore a rod-like shape is retained.

As the viscosity contrast is increased (e.g. $vr \geq 20$–40) and with shear stains where $\gamma > 5$ (e.g. Figs. 4b, 5) the ends of the hard grain begin to rotate. The higher the viscosity contrast (Fig. 4c, d) the more obvious this phenomenon becomes. These regions (Fig. 3e) can be compared with the sites of kinking and/or boudinage observed in the experimental work by Delle Piane et al. (2009). The deformation at the tips of the long grain is a function of its aspect ratio. The harder grains maintain the dimension of their short axes and cause a local change in the velocity fields and a deflection at the tips. For example if we look at the progressive series of experiments in Fig. 4d it is seen that the ends of the isolated hard grain have rotated 90°, with respect to the central region of the grain, at a shear strain of $\gamma = 17.5$ (Fig. 5c). In contrast, the matrix grains away from the hard grain have a strong grain shape foliation that is being progressively elongated and rotated with increasing shear strain without developing any instability between the grains.

Instability in the foliation is developed around the ends and adjacent to the hard grain with increased shear strain (Figs. 4b–d and 5). It is here that there is much more strain localisation in the matrix grains and a progressive concentration around the tip of the

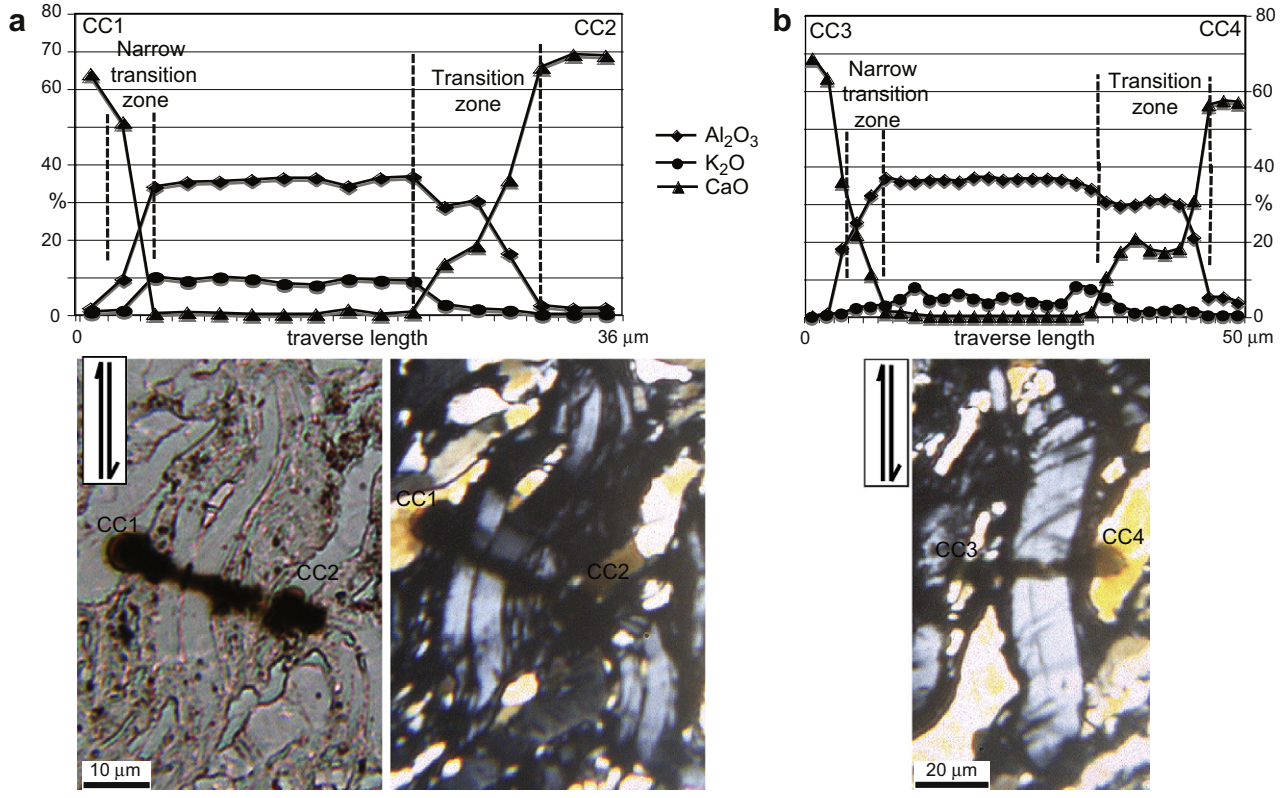

Fig. 3. Compositional profiles of aluminium, potassium and calcium oxides across muscovite porthyroclasts based on microprobe data from sample PO754 of Delle Piane et al. (2009). (a, b) Profile from calcite to calcite grains CC1–CC2 and CC3–CC4 and includes the following parts: calcite, narrow transition, muscovite, wider transition and calcite again. The wider transition is represented by decrease in Al_2O_3 and K_2O and marked increase in CaO and corresponds to the reaction zones illustrated in Fig. 1d, e. (c, d) Location of microprobe damage zone across buckled muscovite in plane-polarised light and crossed nicols that corresponds to profile CC1–CC2. (e) Location of microprobe traverse CC3–CC4 across buckled muscovite that has an increased number of kinks adjacent to its rotated tip (crossed nicols). Note that the wider transition zones in (a, b) are located in the concave sections of the buckled muscovites.

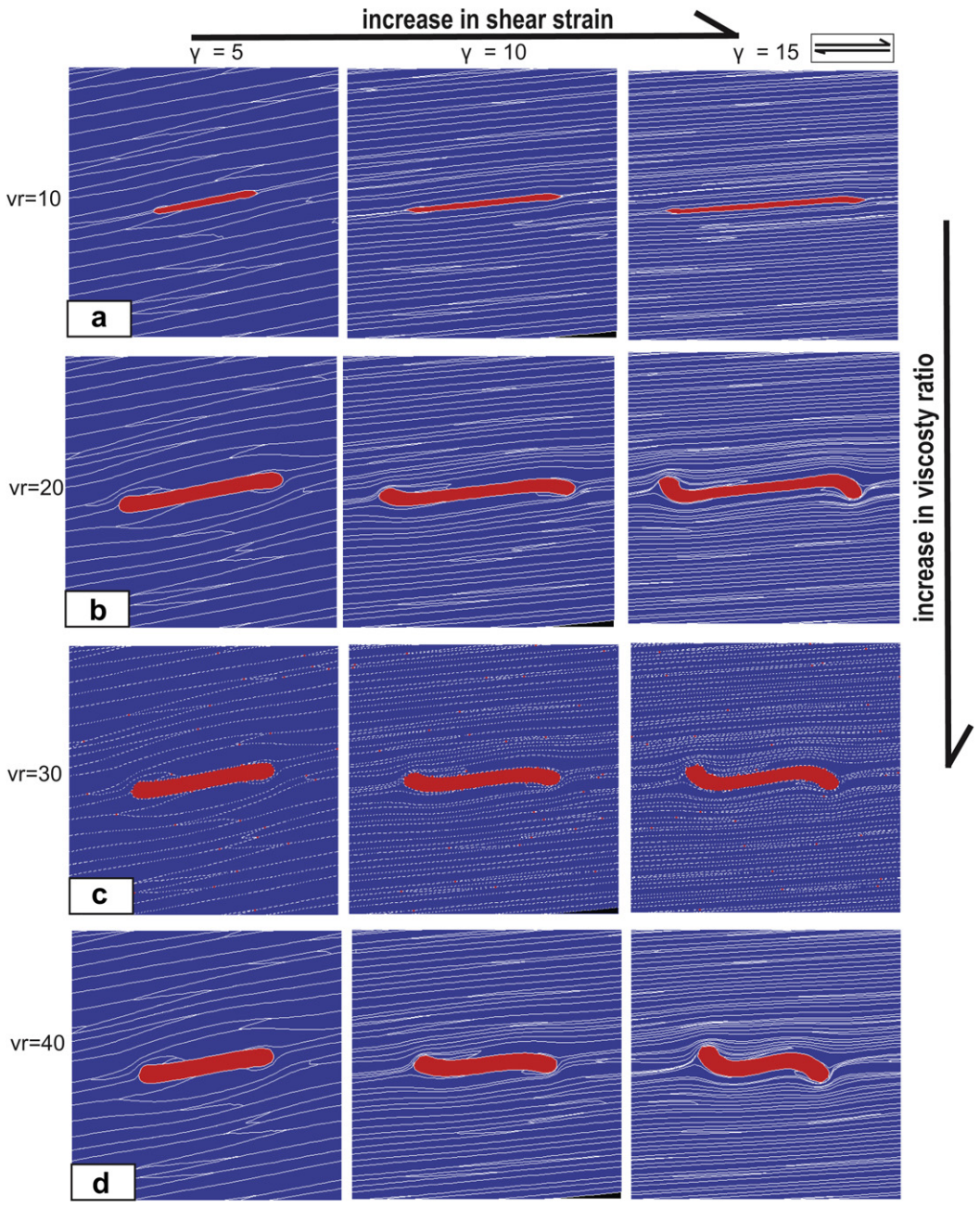

Fig. 4. The sequential evolution for single hard grain (red grain) embedded in ductile matrix (blue grains) with varying viscosity contrasts deformed during a dextral simple shear. The shear strain (γ) is displayed on the horizontal axis and the viscosity contrast (vr) on the vertical axis. (a–d) Models deformed with viscosity contrasts of 10, 20, 30 and 40. The rotation rate of the hard grain slows as the long axis aligns with the shear direction during the progressive deformation. (For interpretation of the references to colour in this figure legend, the reader is referred to the web version of this article.)

rotating hard grain. If we examine the deformed grain mesh (Fig. 4d; $\gamma = 5$) we can see that the elongate shaped grains, which originally had a more equant shape (Fig. 2), are deflected and rotated around the end of the hard grain. As the strain is increased the ends of the hard grain begin to rotate, the matrix grains become more elongate and a clockwise flow pattern begins to be localised close to the ends of the porphyroclast (Fig. 4d; $\gamma = 15$). The clockwise flowing segments are in effect microshear zones that locally partition the flow, in a clockwise sense, with respect to the bulk dextral shear sense. There is a thinning of matrix grains behind the tip of the rotating porphyroclast, whereas, in the lee of the porphyroclast there is a preservation of the already strained matrix grains. This deformation results in a further effective decrease in aspect ratio of the hard grain and it behaves like a more equant porphyroclast with the shape of its enclosing ellipse.

In all these models variation in mean stress is characterised by being compressive in the matrix and tensile or extensional in the hard object. This can be best illustrated in Fig. 6, where the stress exponent was set at 1 and the viscosity contrasts were varied from 10 to 40. We can see that when $\gamma = 2.5$ an elongate foliation evolved in the matrix grains. In the initial stage the long axis is perpendicular to the shear direction, the stress adjacent to the embedded hard grain is asymmetric and the minimum principal stress is compressive in the dextral simple shear direction.

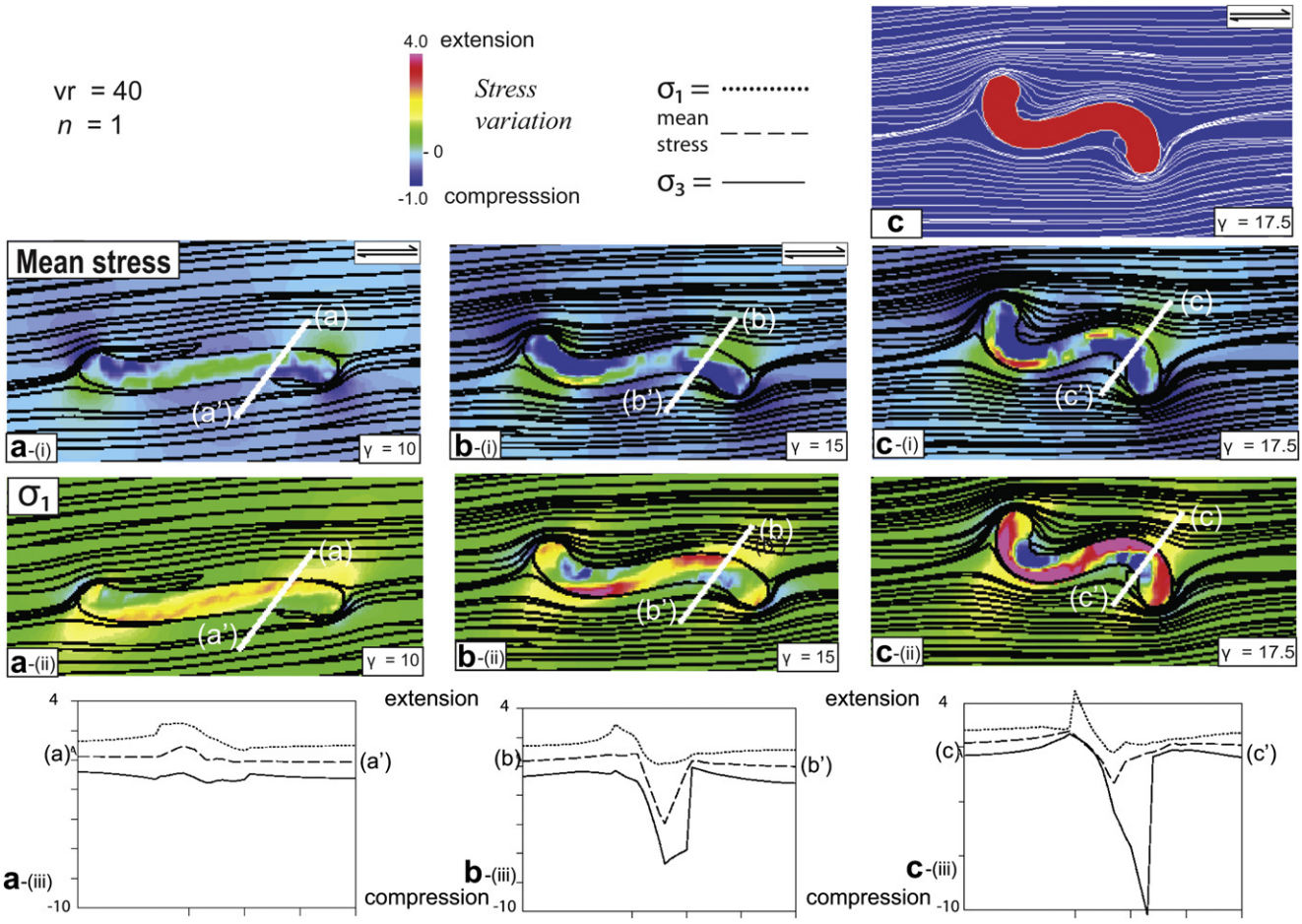

Fig. 5. The stress variations related to a single elongate grain deformed in dextral simple shear with a stress exponent $n = 1$ and viscosity contrast vr = 40. The vertical columns (a) shows a shear strain $\gamma = 10$; (b) shear strain $\gamma = 15$; (c) grain boundary and stress maps at a shear strain $\gamma = 17.5$. The horizontal row (i) shows maps of the mean stress distribution with contours of the average stress and the location of the profiles across the hard grain (ii) maps of σ_1 variations and (iii) individual profiles of σ_1 (dotted line), mean stress (dashed line) and σ_3 (solid line) across the sheared hard grain.

4. Paired porphyroclasts with contrasting matrix viscosities

Figs. 7a and 8a show images of the initial microstructure where there are soft grains in the matrix and two isolated hard grains lying either perpendicular or parallel to the direction of shear. It should be noted that the ends of the hard grain are irregular and represent grains, such as micas, that have equilibrated within a matrix of polygonal grains as in a regionally metamorphosed quartzite or marble (Spry, 1969; Passchier and Trouw, 2005). This is in marked contrast to the rectilinear (e.g. Treagus and Lan, 2003) or elliptical

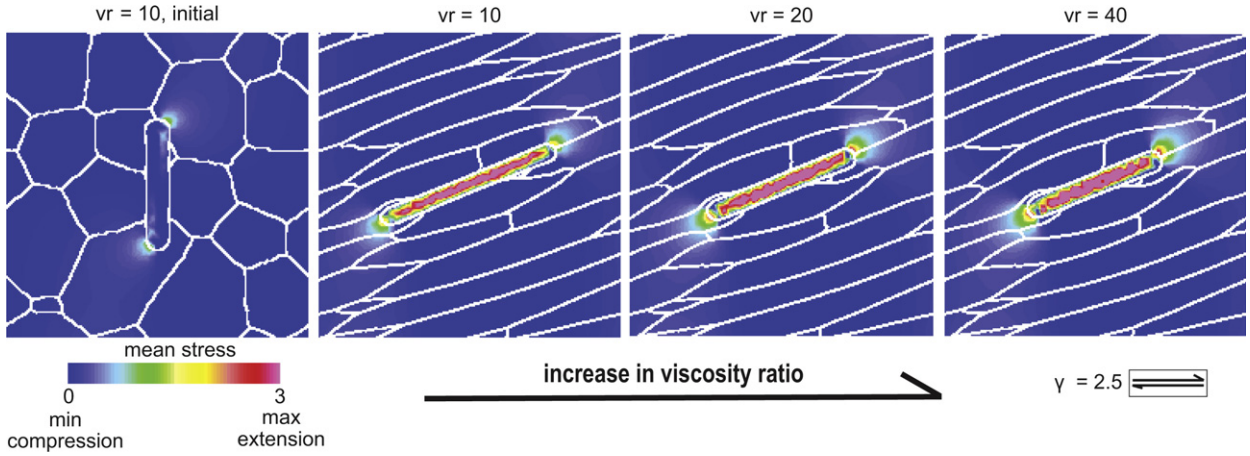

Fig. 6. The evolution and grain boundary map for a single elongate grain deformed in a matrix of polygonal grains with a stress exponent $n = 1$ and the mean stress distribution. The starting microstructure is illustrated on the left and the models are deformed in simple shear ($\gamma = 2.5$) with increasing viscosity contrast (vr = 10, 20 and 40) shown to the right. Green and red colours indicate increasing extension and blue are grains undergoing compression. Note that these are relative and are not absolute values of the mean stress.

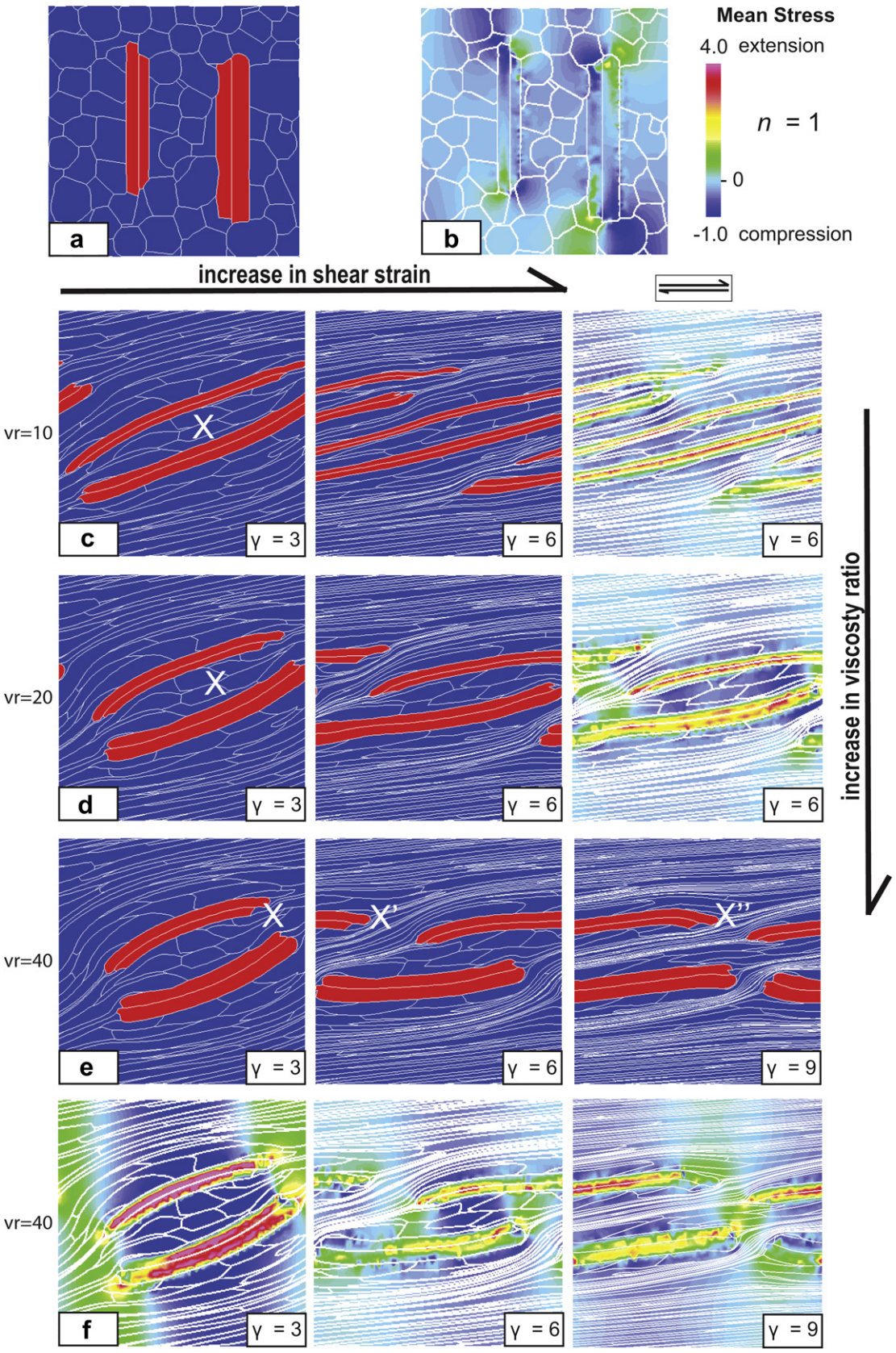

Fig. 7. Dextral shear of two hard grains initially perpendicular to the shear plane in a matrix of softer grains with a stress exponent of $n = 1$. Note the numerical models imposes wrapping of vertical boundaries, so that with increasing strain the hard grain in the upper-right of the model would re-appear on the upper-left hand side. (a) Initial grain configuration. (b) Map of initial mean stress distribution in sample with a viscosity ratio of 10 and scale illustrating the variation from an extensional (red) to compressional regime (blue). (c, d) These rows show the variation in microstructure with viscosity ratios (vr) of 10 and 20, shear strains (γ) of 3 and 6, with the mean stress distribution at $\gamma = 6$. (e, f) Microstructure and corresponding mean stress distributions in sample with vr = 40 and $\gamma = 3$, 6 and 9.

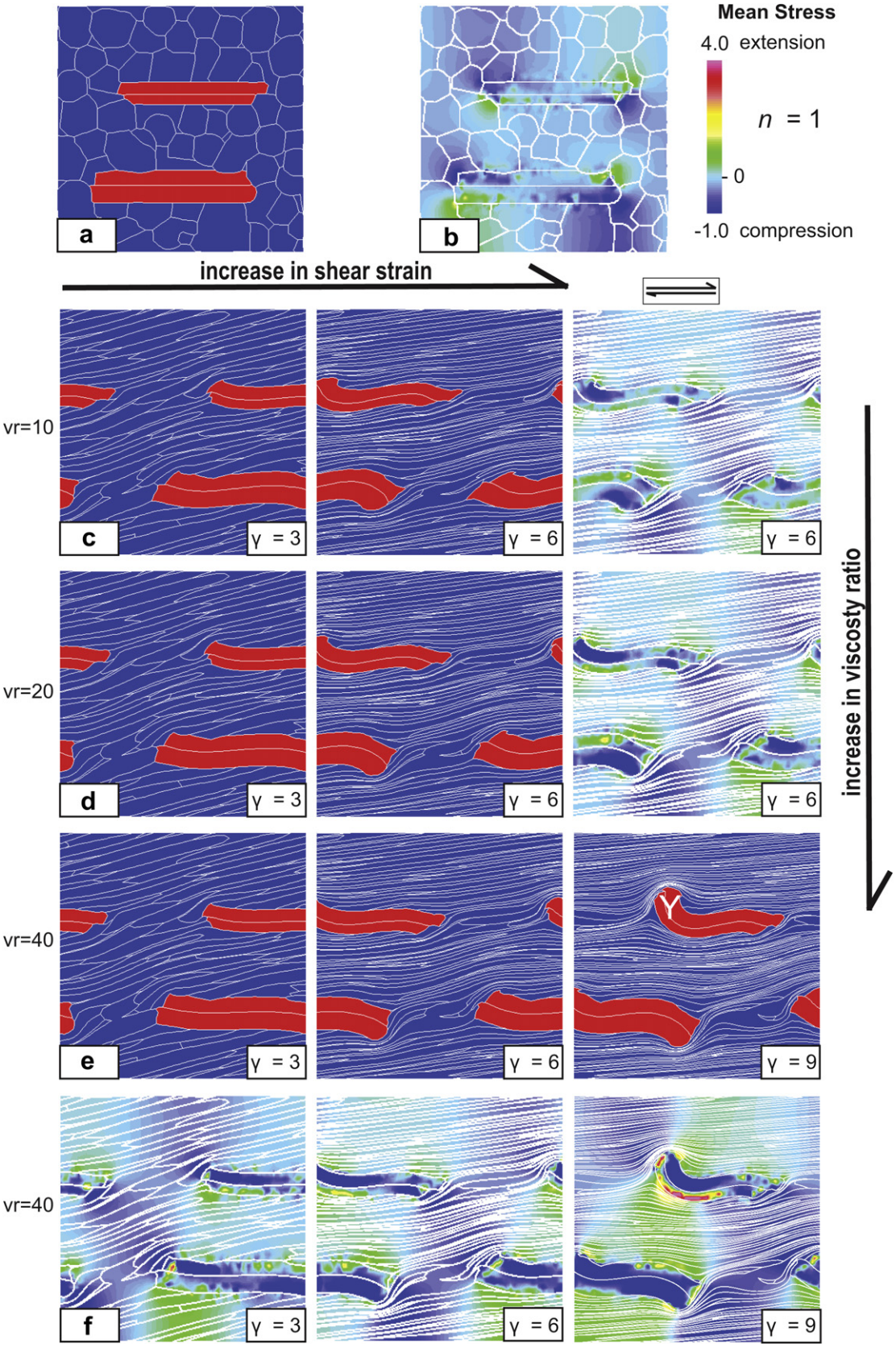

Fig. 8. Dextral shear of two hard grains initially parallel to the shear plane in a matrix of softer grains with a stress exponent of $n = 1$. (a) Initial grain configuration. (b) Map of initial mean stress distribution in sample with a viscosity ratio of 10 and scale illustrating range of variation at $\gamma = 0$. (c, d) These rows show the variation in microstructure for viscosity contrasts (vr) of 10 and 20, shear strains (γ) of 3 and 6, with the mean stress distribution at $\gamma = 6$. (e, f) Microstructure and corresponding mean stress distributions in sample with vr = 40 and $\gamma = 3$, 6 and 9.

configuration (Ceriani et al., 2003) used by previous workers to model the evolution of porphyroclasts.

In all of the current models the soft matrix grains distal to the two hard grains, show little variation from what is seen in the single porphyroclast models, they simply elongate and rotate with increasing strain. The stress–strain patterns vary with the distribution of hard grains so that, in addition to rotation, lateral changes cause local perturbations in the foliation. Similarly the region adjacent to and between the two rotating hard grains can become an area of foliation instability and varies significantly depending if the grains were originally lying at a high-angle (Fig. 7a) or parallel to the shear direction (Fig. 8a) and these differences are considered separately.

4.1. Paired porphyroclasts perpendicular to shear direction

Hard grains oriented at a high-angle to the direction of shear (Fig. 7a) have an initial low mean stress that is comparable to the matrix grains (Fig. 7b). With a viscosity contrast of vr = 10 (Fig. 7c) there is a marked elongation of the hard grains with increasing shear strain similar to that observed with a single porphyroclast (Fig. 4). The map (Fig. 7c; $\gamma = 6$) that displays the mean stress distribution within the matrix grains is compressional, whereas, the hard grains have a core in extension bounded by a transitional zone that grades into the compressive regime of the matrix grains.

At shear strains of $\gamma = 3$ and viscosity contrasts of 20 and 40 (Fig. 7d, e) the hard grains undergo less extension and begin to buckle. These buckles curve inward about a core of less strained matrix grains (area X in Fig. 7d, e) with their outer margin also flanked by elongate matrix grains that pass out into the highly deformed distal matrix grains. Further shear strain ($\gamma = 6$) is then accommodated by continued rotation of the buckled grains, without amplification of the buckles, and the localisation of strain adjacent to the ends of the hard grains. These terminations of the paired hard grain also begin to rotate at shear strains $\gamma \geq 9$ (Fig. 7e) in a fashion comparable to the single porphyroclasts observed at shear strains of $\gamma \geq 10$ (Figs. 4 and 5).

Once the paired hard grains are rotated into near parallelism with the shear plane (Fig. 7e) then the area of relatively unstrained grains (e.g. at X Fig. 7e; $\gamma = 3$) is progressively deformed with increasing shear strain. The hard grains begin to separate (area X′ Fig. 7e; $\gamma = 6$) and eventually this becomes a region of intense strain localisation with the development of a prominent foliation (area X″ Fig. 7e; $\gamma = 9$). The accompanying map of mean stress distribution in the hard grains is dominantly tensional at $\gamma = 3$ (Fig. 7f) becoming weaker and more diffuse with increasing shear (Fig. 7f; $\gamma = 9$).

4.2. Paired porphyroclasts parallel to shear direction

The behaviour of the hard grains, with low viscosity contrasts (vr = 10, 20) and initial lengths lying parallel to the shear direction buckles with little rotation or elongation (Fig. 8c, d). There are insignificant variations in the distribution of mean stress and a near uniform variation of strain between the hard and matrix grains. This is in marked contrast to the situation where the initial hard grains were perpendicular to the shear plane (Fig. 7c, d); the latter displayed significant elongation and an inhomogeneous distribution of strain in the matrix grains and significant variations in mean stress.

With higher viscosity contrasts (vr = 40) and higher shear strains ($\gamma = 9$) the termination of the hard grains (Y in Fig. 8e) begins to rotate towards the shear direction. The deformation in the soft matrix grains is then partitioned into two regions: (1) on the outside of the hard grain, where intense deformation and presumably strain softening processes are occurring and (2) a tail behind the porphyroclast, where grains are undergoing less deformation and their shape does not reflect the bulk shear strain. At these higher strains (Fig. 8f; $\gamma = 9$) a band of significant extension spreads across the model between and adjacent to the two hard grains with a significant increase in extension adjacent to the outer arc of greatest buckling in the hard grain. This mean stress variation (Fig. 8f; $\gamma = 9$) at the point of greatest buckling is highly asymmetric with the core of the hard grain undergoing more compression than the adjacent matrix grains.

5. Stress variations between matrix and porphyroclast

In experiments involving increasing viscosity contrasts in the single porphyroclast models we saw that maps of the mean stress variation (Figs. 5 and 6), always showed extensional stresses in the core of the hard grain. As the hard grain rotated from the shortening field into the finite extension direction (Fig. 2c), higher mean stresses were observed in the hard grain with lower stresses observed at its interface with the matrix (Fig. 6). This produces a region of tensile stress at the interface, which is a function of substantially lower σ_1 in that part of the model. All that is required is for the elongate grain to be slightly stiffer (i.e. higher viscosity contrast) than the matrix grains.

With higher viscosity contrasts and increasing shear strains the stress distribution maps show changes along the length of the hard grain as it progressively buckles (Fig. 5). The mean stress in the inner arcs becomes more compressive [Fig. 5a-(i)–c-(i)], whereas, the distribution of σ_1 becomes strongly extensional at shear strains of $\gamma = 17.5$ [Fig. 5c-(ii)]. This transition and the increasing asymmetry in the σ_1 and σ_3 stress distribution across the grains clearly seen in the profiles [Fig. 5a-(iii)–c-(iii)], with one grain interface being in compression and the other in extension.

As seen in the contour maps in Figs. 7 and 8 the distribution of mean stress in the paired porphyroclast models was highly variable and dependant on the initial orientation of the hard grains. The mean stresses developed during the deformation of the perpendicular models (Fig. 7) showed the greatest variation, with areas of slightly compressive stresses in the shortening field and in the region of matrix grains between the two rotating hard grains. To investigate this further a series of models were developed to look at the sequential evolution and variation of stress between the matrix and the hard grains (Fig. 9). Three profiles were constructed perpendicular to one of the hard grains seen in the mean stress maps, in a plane that approximately parallels the maximum principal stress direction (σ_1).

In detail this stress variation at the boundary of the hard grain becomes more accentuated with increasing shear strains and nonlinearity (increasing exponents of n). The distribution of the mean stress [Fig. 9, column (i)] shows an increasing concentration of the extensional stresses into the region between and adjacent to the two hard grains as the exponents n increases [Fig. 9, columns a(i)–e(i)]. What is most distinct about this central region is the asymmetry of the increasing tensional nature of the inward facing interface of the two porphyroclasts. If profiles of mean stress are compared along the length of the hard grain [Fig. 9, column (ii)] it is noticed that there are subtle variations along the length at the grain boundary interface, but there are striking similarities in pattern between individual profiles. These are characterised by marked increases of the extensional stress in the core of the hard object with increased contraction on the grain interface. The distribution of mean stresses also changes symmetry with respect to incremental strain and exponents n, as shown by the shape changes in the profiles [Fig. 9, columns a(ii)–e(ii)].

Similar asymmetric patterns are observed in the distribution of the maximum (σ_1) and minimum (σ_3) principal stress [Fig. 9, columns (iii), (iv) and (v)] in each of the individual profiles with

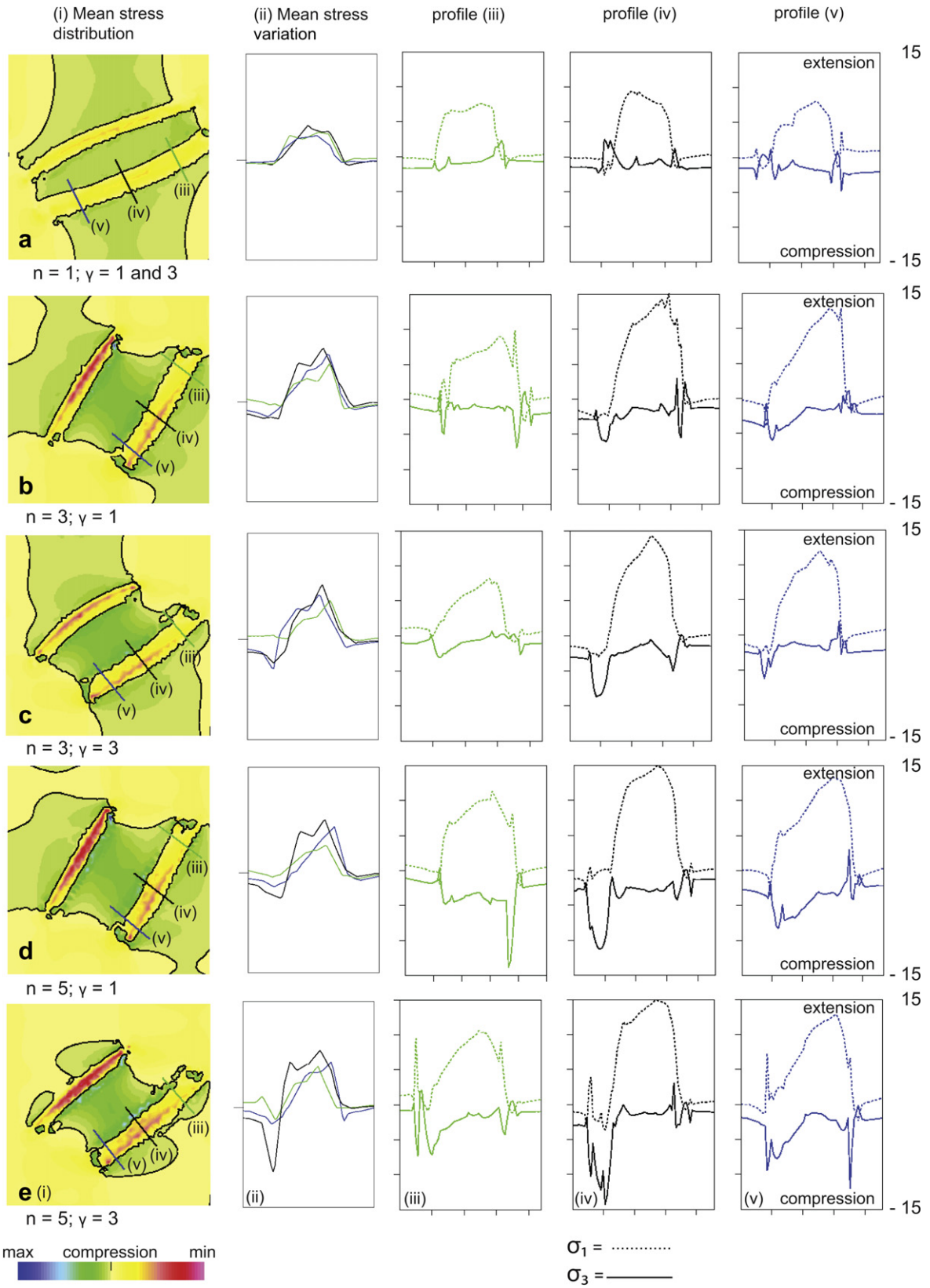

Fig. 9. Stress components related to varying viscosities and shear strain in the paired grain models initially perpendicular to the shear direction. (a) $n = 1$, $\gamma = 1$ and 3. The stress distribution maps and profiles for $\gamma = 1$ and 3 are almost identical; (b) $n = 3$, $\gamma = 1$; (c) $n = 3$, $\gamma = 3$; (d) $n = 5$, $\gamma = 1$; (e) $n = 3$, $\gamma = 1$. Each horizontal row shows (i) map of the mean stress distribution with contours of the average stress and the location of the profiles across the hard grain (ii) profiles of mean stress (iii–v) individual profiles of σ_1 (dotted line) and σ_3 (solid line) across the sheared hard grain. At higher values of n and γ there are increasing variations in stress at the interface between the hard grain and soft matrix.

increasing incremental strain and the exponent n. There is a zone of higher compressive stress on the inboard side of the two hard grains and at their ends. This change is particularly marked in the centre of the hard grain [Fig. 9, column (iv)] and in the magnitude of σ_3, but there is little variation in σ_1. If the deformation mechanism had been linear viscous, i.e. stress exponent $n = 1$ (Fig. 9, row a) then σ_3 at the interface between the matrix grains and hard grain would be tensional [Fig. 9a(iv)]. However, this is not the case for the non-linear viscous distribution considered in our models, as n and γ increase there is asymmetric localisation and concentration of the σ_3 becoming more compressive on the inboard side of the hard grain boundary [Fig. 9, column (iv) rows b–e]. This pattern is also strongly reflected in the increasing and more asymmetric parabolic distributions of mean stress as n and γ increases [Fig. 9, column (ii) rows b–e].

6. Comparison with the stress variation during pure shear

If the hard grain was oriented perpendicular to the shear direction, in a pure shear regime, then there is a non-rotational component to the strain, and the mean stress will be nearly uniform along the grain (Fig. 10a, b). The magnitude of the tensile stress σ_3 would be high (Fig. 10c) and σ_1 would be uniform (Fig. 10d, f). If we assume the hard grain is a muscovite with (001) parallel to the long axis of the grain. Then this means that in a pure shear regime, the hard grain would preferentially crack along its axis, and there would be no areas of differential stress along the grain boundary to drive dehydroxylation reactions of the type described by Mariani et al. (2006). Therefore the highly compressive stresses seen across the grain (Fig. 10c) would also explain the lack of reaction products seen in the compression experiment described by Delle Piane et al. (2009).

7. Discussion

7.1. Effects of contrasting matrix framework and viscosities

The hard grains used in these models were non-equant with a marked viscosity contrast to their matrix grains. In doing so, we recognise that with small shear strain simulations ($\gamma < 2$), hard grains begin to deform by buckling with the localisation of deformation controlled by their degree of rotation. However, the nature of the deformation is influenced by three main parameters: (1) the viscosity contrast between the hard grain and its weak matrix grains; (2) orientation of the long axis to the shear plane; and (3) the volume and spatial distribution of the weak material between the hard grains. The weak phase forms interconnected layers subparallel to the shearing plane except close to the embedded hard grain. Unlike previous studies (ten Grotenhuis et al., 2002; Ceriani et al., 2003) the grain boundary interfaces in these models could not undergo any brittle displacement, with all grains undergoing a fully plastic deformation. Such intracrystalline deformation is the type of fully viscous flow that you would expect in the earth's middle crust, where the mechanical properties of muscovite (Bell and Wilson, 1981) are highly anisotropic compared to all other common rock forming minerals (Johnson et al., 2004).

The numerical experiments of grains initially perpendicular to the shear plane produced very consistent results concerning the influence of initial orientation on the subsequent rotation of the hard grain. All hard grains with low viscosity contrasts underwent extension as they were rotated into the plane of shear. This grain extension diminished rapidly, as the viscosity contrast increased, and was accompanied by a greater buckling and rotation of the hard grain. Higher viscosity contrast resulted in extensive deformation initiating in the neighbouring matrix (Fig. 7e) with high shear strain, with grain extension occurring in the matrix grains adjacent to the hard grain as the latter was progressively rotated.

In the grains initially parallel to the shear plane there was little extension in the hard grain and most of the deformation was confined to the matrix grains and the results are similar to those described by Johnson et al. (2004). However, in the tail of the resulting porphyroclast there is a 'pressure shadow' effect with the preservation of less deformed grain shapes and sizes (Fig. 8). This latter feature was also noted at much higher shear strains ($\gamma \leq 15$) in the single hard grain models (Fig. 4) where the matrix continues to flow undisturbed until the long axis of the hard grain has passed through the shear plane and rotates towards the shear direction (Figs. 4d and 5). In the paired models as the grains move laterally with respect to each other the strain patterns change and may initiate rotation, with dynamic changes locally without any variation in boundary conditions. This can be seen as diagonal regions with different mean stress, linked by the two hard grains that transect the matrix oblique to the shear plane (e.g. Fig. 8f) similar to the differential stress partitioning described by Johnson et al. (2004).

7.2. Stress variation and implications for diffusion processes

Stress-induced diffusion is accommodated by a net flux of material from high- to low-stress interfaces. For instance Wheeler and Ford (2008) point out that it is not the stress inside a grain that drives diffusion; it is only the normal stress gradients in the interface regions. In these numerical models the high mean stress distributions were coincident with the tails of the porphyroclasts and localised to the elongate boundaries of the hard grain. This is in marked contrast to hard grain interiors where there are higher tensile stresses. However, by comparing σ_3 in similarly oriented grains with increasing non-linear behaviour (Fig. 9b–e) it is seen that σ_3 is not symmetrically distributed along a grain boundary and becomes strongly asymmetric as n increases. A similar observation is also noted with increasing shear strain in the single porphyroblast models (Fig. 5).

The microstructures also suggest that there is a marked difference in the stress/strain distribution depending on the initial orientation of the porphyroclasts. The hard grains initially parallel to the shear plane, remain oriented with their long axes aligned in the shear direction. There are small areas of higher stress and the shear strain is concentrated in the matrix layers between the hard grains, indicated by the closely spaced, elongated boundaries. The hard grains that were initially perpendicular to the shear flow have rotated ($\gamma > 6$) and there is some horizontal translation of the pophyroclasts. The matrix grains in close proximity and especially those between the porphyroclasts are in low-stress regions, where there would be less strain induced recrystallisation. In contrast, the areas of high shear strain would be regions of small recrystallised grains with a dense network of grain boundaries. Grain boundary diffusion would be faster in these networks (Park et al., 2004) than in the unrecrystallised areas, making them preferential sites for reaction products. The higher tensional stress in the deformed porphyroclasts would provide a strong stress gradient at the matrix interface while the variation in grain size would provide a diffusion gradient in the matrix e.g. in the region distal to the hard grains.

7.3. Comparison of results with previous experiments and natural examples

The natural equivalent of the hard grain would be a stronger phase such as muscovite with its basal plane oblique to a weak layer (Fig. 1a). We believe that the modelling is able to reproduce many of the features observed in natural rocks. Particularly where the

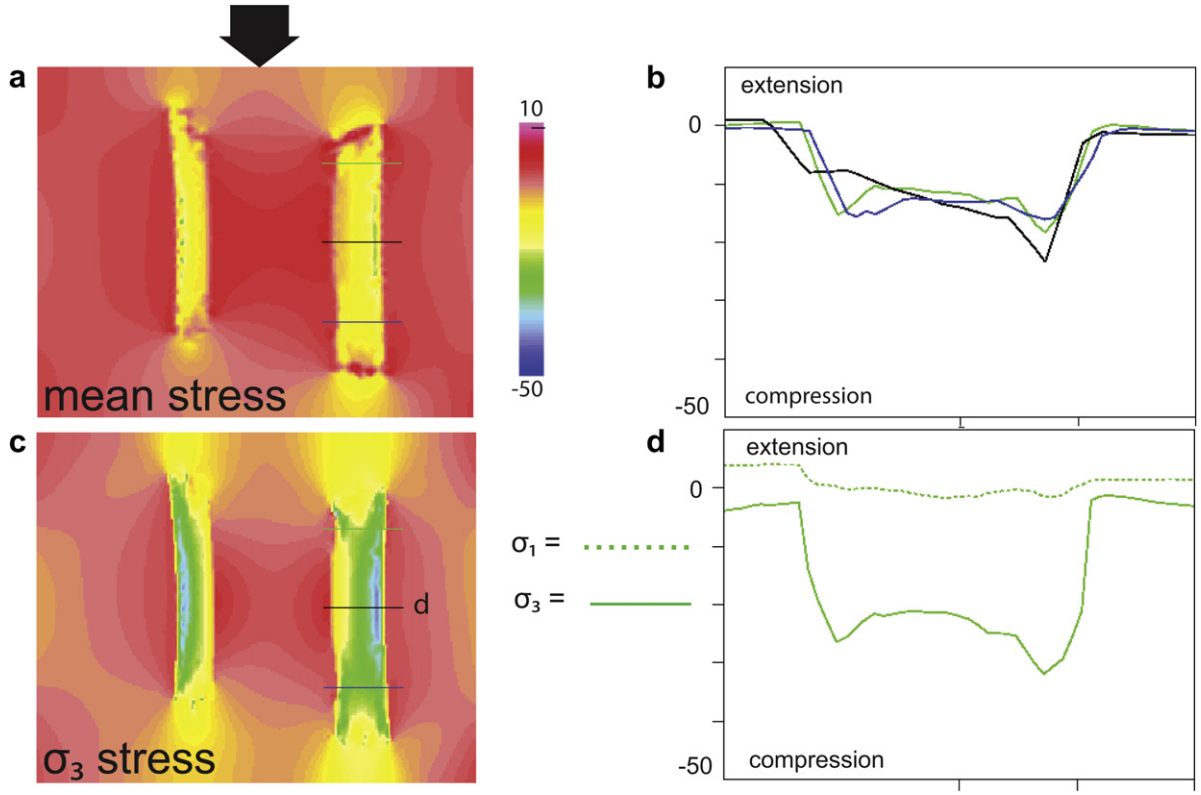

Fig. 10. Stress variation in two hard grains where vr = 20 after a 10% pure shear shortening. (a, b) Mean stress distribution map with profiles across hard grain and scale illustrating the variation from an extensional (red) to compressional regime (blue). (c) Map of σ_3 stress distribution. (d) Example of σ_1 (dotted line) and σ_3 (solid line) profiles that illustrates the strong compressional stress across the hard grain.

deformation is constrained to the matrix and the muscovite is not dominated by slip along cleavage planes of the muscovite crystal. This would not be the case if the rock contains small volumes of a weaker phase such as biotite, that readily recrystallises. Where adjacent muscovite fish are observed in natural rocks (e.g. Fig. 1b) the muscovite is bent and curves inward and has microstructures very comparable to the range of deformation patterns observed in Figs. 7 and 8, and always lie in the extensional field of the finite strain ellipse. However, in nature there is also the complication of having grain boundary sliding and the effects of recrystallisation both in the muscovite and in the matrix grains, something that is not considered in these numerical simulations.

In the high shear strain experiments of Mariani et al. (2006) and Delle Piane et al. (2009) the bending of the muscovite grains and a zonation of reaction products (Fig. 3), appears to be strongly related to the shape and position of the muscovite in the shear field (Fig. 2c). Muscovite grains at shear strains of $\gamma = 1$ (Fig. 1c) did not undergo reaction, whereas, grains where $\gamma \geq 2$ were accompanied by asymmetric reaction rims (Fig. 1d, e). An explanation for this observation is that the areas of reaction products correspond to areas near muscovite boundaries with large minimum stress gradients (Figs. 5, 7–9). High tensile stress would cause boudinage and micropores in the muscovite allowing dehydroxylation and exchange reactions.

In the experiments of Delle Piane et al. (2009) a region up to 12 μm wide adjacent to the muscovite is heterogeneously enriched in CaO and decreased in Al_2O_3 and K_2O (Fig. 3) and a complex zoning pattern is developed (Fig. 2d, e) that, in metamorphic rocks, would normally be interpreted in terms of changes in average pressure or temperature or episodic fluid infiltration. These explanations cannot apply to our experiments, instead the zoning pattern is interpreted as being due to diffusion driven by variations in the least minimum stress. Enhanced diffusion in such stressed boundaries in combination with the build up of intracrystalline defect energy in the deformed grain can be a driving force for the nucleation of new phases and grain boundary migration. The possibility that diffusion involving external fluids in stressed grain boundaries might be much faster, e.g. pressure solution, has been the subject of extended debate in the geological literature. The fact that significant variation in minimum stress is only seen at high values of n and γ suggests that the rearrangement of dislocations could also facilitate the enhanced rates of diffusion.

Therefore our numerical simulations suggest there is a feedback relationship between stress partitioning at high shear strains and metamorphic reaction. The existence of pressure shadows, strain fringes in rocks all testify to the existence of local stress fluctuations. We have shown that small differential stresses within high-strain zones, involving phases with contrasting viscosities, can lead to local disequilibrium with respect to pressure (and temperature) and the rapid advection of reactant components. The magnitude of the local differential stress around the porphyroclast is a function of both the viscosity contrast and the stress exponent n (Fig. 9). This probably explains the microstructural observation that many reaction coronas observed around porphyroclasts (Passchier and Trouw, 2005) may be the consequence of strain localisation and reflects the local stress field rather than a thermal perturbation or a product of separate metamorphic decompression reactions.

8. Conclusions

The rotations and processes related to the porphyroclast evolution in the numerical simulations are directly comparable to the calcite–muscovite experiments undertaken by Delle Piane et al. (2009). Mechanical strengths of individual hard grains in

a matrix of soft grains were varied by systematically changing the viscosity contrast. The difference in initial orientation and viscosities between the grains led to distinct partitioning of the micromechanical deformation characteristics. Hard grains initially parallel to the shortening direction are rapidly rotated into the extensional field. When these grains reach a low-angle to the shear direction, the grains are in a stable state and buckling at their ends becomes the dominant mode of deformation at higher shear strains. Associated with this buckling is a localised decrease in the minimum principal stress at the porphyroclast interface, so that it is significantly different from the average mean stress in the grain aggregate.

The influence of viscosity contrast is not as obvious in hard grains that were initially parallel to the finite extension direction; these tend to maintain a stable position with increasing buckling at higher values of shear strain. The stability of the porphyroclasts in this orientation allows interconnected flow patterns to develop in the matrix. However, at high values of shear strain significant localised deviations of minimum principal stress from the mean stress are developed at grain interfaces. It is the development of these increasing tensile stresses at the grain interface that probably leads to the enhancement of diffusion controlled processes at the grain boundary. The variations in mean stress, attributable to changes in the minimum principal stress, could account for the complex mineral zoning patterns observed in highly sheared metamorphic rocks.

Acknowledgements

This research was supported by an Australian Research Grant DP0773097. The authors are grateful to Mark Jessell, Paul Bons, Jens Becker and Greg Houseman for their work on successive versions of the Elle software and BASIL. Luigi Burlini is thanked for his support and contributions to the calcite–muscovite experimental studies and our initial discussions about the role of stress in enhancing metamorphic reactions in a simple shear regime. Mark Jessell, Scott Johnson and an anonymous referee are thanked for their valuable comments on this work.

References

Arbaret, L., Mancktelow, N.S., Burg, J.-P., 2001. Effect of shape and orientation on rigid particle rotation and matrix deformation in simple shear flow. Journal of Structural Geology 23, 113–125.
Barr, T.D., Houseman, G.A., 1996. Deformation fields around a fault embedded in a non-linear ductile medium. Geophysics Journal International 125, 473–490.
Barnhoorn, A., Bystricky, M., Burlini, L., Kunze, K., 2004. The role of recrystallisation on the deformational behaviour of calcite rocks: large strain torsion experiments on Carrara marble. Journal of Structural Geology 26, 885–903.
Barnhoorn, A., Bystricky, M., Kunze, K., Burlini, L., Burg, J.-P., 2005. Strain localisation in bimineralic rocks: experimental deformation of synthetic calcite-anhydrite aggregates. Earth and Planetary Science Letters 240, 748–763.
Bell, I.A., Wilson, C.J.L., 1981. Deformation of biotite and muscovite: TEM microstructure and deformation model. Tectonophysics 78, 201–228.
Bons, P.D., Koehn, D., Jessell, M.W., 2008. Microdynamics Modelling. Springer, Berlin.
Casey, M., 1980. Mechanics of shear zones in isotropic dilatant materials. Journal of Structural Geology 2, 143–147.
Ceriani, S., Mancktelow, N.S., Pennacchioni, G., 2003. Analogue modelling of the influence of shape and particle/matrix interface lubrication on the rotational behaviour of rigid particles in simple shear. Journal of Structural Geology 25, 2005–2021.
Dell'Angelo, L.N., Tullis, J., 1988. Experimental deformation of partially melted granitic aggregates. Journal of Metamorphic Geology 6, 495–515.
Dell'Angelo, L.N., Tullis, J., Yund, R.A., 1987. Transition from dislocation creep to melt-enhanced diffusion creep in fine-grained granitic aggregates. Tectonophysics 139, 325–332.
De Bresser, J.H.P., Spiers, C.J., 1997. Strength characteristics of the *r*, *f*, and *c* slip systems in calcite. Tectonophysics 272, 1–23.
Delle Piane, C., Burlini, L., 2008. Influence of strain history on the mechanical and micro-fabric evolution of calcite rocks: insights from torsion experiments. Swiss Journal of Geosciences 101, 361–375.
Delle Piane, C., Wilson, C.J.L., Burlini, L., 2009. Dilatant plasticity in high-strain experiments on calcite–muscovite. Journal of Structural Geology 31, 1084–1099.
Eisbacker, G.H., 1970. Deformation mechanisms of mylonitic rocks and fractured granulites in Cobequid Mountains, Nova Scotia, Canada. Geological Society of America Bulletin 81, 2009–2020.
Etheridge, M.A., Hobbs, B.E., Paterson, M.S., 1973. Experimental deformation of single crystals of biotite. Contributions to Mineralogy and Petrology 38, 21–36.
Evans, B., Hay, R.S., Shimizu, N., 2001. Diffusion-induced grain-boundary migration in calcite. Geology 14, 60–63.
Evans, L., Jessell, M.W., Bons, P.D., Koehn, D., 2008. Introduction to Elle. In: Bons, P.D., Koehn, D., Jessell, M.W. (Eds.), Microdynamics Modelling. Springer, Berlin, pp. 77–85.
Handy, M.R., Wissing, S.B., Streit, L.E., 1999. Frictional-viscous flow in mylonite with varied bimineralic composition and its effects on lithospheric strength. Tectonophysics 303, 175–191.
Herwegh, M., Jenni, A., 2001. Granular flow in polymineralic rocks bearing sheet silicates: new evidence from natural examples. Tectonophysics 332, 309–320.
Holyoke, C.W.I.I.I., Tullis, J., 2006. Mechanisms of weak phase interconnection and the effects of phase strength contrast on fabric development. Journal of Structural Geology 28, 621–640.
Houseman, G.A., Barr, T.D., Evans, L., 2008. Basil: stress and deformation in a viscous material. In: Bons, P.D., Koehn, D., Jessell, M.W. (Eds.), Microdynamics Modelling. Springer, Berlin, pp. 139–154.
Jackson, I., Faul, U.H., Fitz Gerald, J.D., Morris, S.J.S., 2006. Contrasting viscoelastic behavior of melt-free and melt-bearing olivine: implications for the nature of grain-boundary sliding. Materials Science and Engineering A 442, 170–174.
Jeffery, G.B., 1992. The motion of ellipsoidal particles immersed in a viscous fluid. Proceedings of the Royal Society of London A 102, 161–179.
Jessell, M.W., Bons, P.D., Evans, L., Barr, T., Stüwe, K., 2001. Elle: a micro-process approach to the simulation of microstructures. Computers and Geosciences 27, 17–30.
Jessell, M.W., Siebert, E., Bons, P.D., Evans, L., Piazolo, S., 2005. A new type of numerical experiment on the spatial and temporal patterns of localization of deformation in a material with a coupling of grain size and rheology. Earth and Planetary Science Letters 239, 309–326.
Jessell, M.W., Bons, P.D., Griera, A., Evans, L., Wilson, C.J.L., 2009. A tale of two viscosities. Journal of Structural Geology 31, 719–736.
Johnson, S.E., 2008. Strain localisation and rigid-object kinematics. In: Bons, P.D., Koehn, D., Jessell, M.W. (Eds.), Microdynamics Modelling. Springer, Berlin, pp. 247–253.
Johnson, S.E., Vernon, R.H., Upton, P., 2004. Foliation development and progressive strain-rate partitioning in the crystallizing carapace of a tonalite pluton: microstructural evidence and numerical modelling. Journal of Structural Geology 26, 1845–1865.
Lister, G.S., Snoke, A.W., 1984. S–C mylonites. Journal of Structural Geology 6, 616–638.
Mancktelow, N.S., 2002. Finite-element modelling of shear zone development in viscoelastic materials and its implications for localisation of partial melting. Journal of Structural Geology 24, 1045–1053.
Mancktelow, N.S., 2006. How ductile are ductile shear zones. Geology 34, 345–348.
Mares, V.M., Kronenberg, A.K., 1993. Experimental deformation of muscovite. Journal of Structural Geology 28, 1569–1587.
Mariani, E., Brodie, K.H., Rutter, E.H., 2006. Experimental deformation of muscovite shear zones at high temperatures under hydrothermal conditions and the strength of phyllosilicate-bearing faults in nature. Journal of Structural Geology 28, 1569–1587.
Marques, F.O., Schmid, D.W., Andersen, T.B., 2007. Applications of inclusion behaviour models to a major shear zone system: the Nordfjord-Sogn detachment zone in western Norway. Journal of Structural Geology 29, 1622–1631.
Means, W.D., 1976. Stress and Strain: Basic Concepts of Continuum Mechanics for Geologists. Springer-Verlag, New York.
Park, Y., Park, D., Evans, L., Ree, J.H., 2004. An Elle-based 2D model for cation exchange reaction between garnet and biotite. Journal of Virtual Explorer 15. http://virtualexplorer.com.au/journal/2004/15.
Passchier, C.W., Trouw, R.A.J., 2005. Microtectonics, second ed. Springer, Berlin.
Pieri, M., Burlini, L., Kunze, K., Olgaard, D., Stretton, I., 2001. Dynamic recrystallisation of Carrara marble during high temperature torsion experiments. Journal of Structural Geology 23, 1393–1413.
Ranalli, G., 1995. Rheology of the Earth, second ed. Chapman and Hall, London.
Rutter, E.H., 1995. Experimental study of the influence of stress, temperature and strain on the dynamic recrystallisation of Carrara marble. Journal of Geophysical Research 100, 24651–24663.
Rybacki, E., Paterson, M.S., Wirth, R., Dresen, G., 2003. Rheology of calcite–quartz aggregates deformed to large strain in torsion. Journal of Geophysical Research 108, 2089. doi:10.1029/2002JB0011833.
Schmid, S.M., Paterson, M.S., Boland, J.N., 1980. High temperature flow and dynamic recrystallisation in Carrara marble. Tectonophysics 65, 245–280.
Shewchuk, J.R., 2002. Delaunay refinement algorithms for triangular mesh generation. Computational Geometry: Theory and Applications 22, 21–74.
Spry, A., 1969. Metamorphic Textures. Pergamon Press, Oxford.
Stüwe, K., 2007. Geodynamics of the Lithosphere. Springer, Berlin.
Tenczer, V., Stüwe, K., Barr, T.D., 2001. Pressure anomalies around cylindrical objects in simple shear. Journal of Structural Geology 23, 777–788.

ten Grotenhuis, S.M., Passchier, C.W., Bons, P., 2002. The influence of strain localisation on the rotational behaviour of rigid objects in experimental shear zones. Journal of Structural Geology 24, 485–499.

ten Grotenhuis, S.M., Trouw, R.A.J., Passchier, C.W., 2003. Evolution of mica fish in mylonitic rocks. Tectonophysics 372, 1–21.

Ter Heege, J.H., De Bresser, J.H.P., Spiers, C.J., 2002. The influence of dynamic recrystallisation on the grain size distribution and rheological behaviour of Carrara marble deformed in axial compression. In: De Meer, S., Drury, M., De Bresser, J.H.P., Pennock, G.M. (Eds.), Deformation Mechanism, Rheology and Tectonics: Current Status and Future Perspectives. Geological Society of London Special Publication, vol. 200, pp. 331–353.

Treagus, S.H., Lan, L., 2003. Simple shear of deformable square objects. Journal of Structural Geology 25, 1993–2003.

Tullis, T.E., Horowitz, F.G., Tullis, J., 1991. Flow laws of polyphase aggregates from end-member flow laws. Journal of Geophysical Research 96, 8081–8096.

Walker, A.N., Rutter, E.H., Brodie, K.H., 1990. Experimental study of grain size sensitive flow of synthetic, hot pressed calcite rocks. In: Knipe, R.J., Rutter, E.H. (Eds.), Deformation Mechanisms, Rheology and Tectonics. Geological Society Special Publication, vol. 54, pp. 259–284.

Wheeler, J., Ford, J., 2008. Diffusion creep. In: Bons, P.D., Koehn, D., Jessell, M.W. (Eds.), Microdynamics Modelling. Springer, Berlin, pp. 161–169.

Wilson, C.J.L., 1975. Preferred orientation in quartz ribbon mylonites. Geological Society of America Bulletin 86, 968–974.

Wilson, C.J.L., Zhang, Y., 1994. Comparison between experiment and computer modelling of plane strain simple shear ice deformation. Journal of Glaciology 40, 46–55.

Wilson, C.J.L., Zhang, Y., Stüwe, K., 1996. The effects of localized deformation on melting processes in ice. Cold Regions Science and Technology 24, 177–189.

Zhang, Y., Jessell, M.W., Hobbs, B.E., 1996. Experimental and numerical studies of the accommodation of strain incompatibility on the grain scale. Journal of Structural Geology 16, 1315–1325.